Catena 207 (2021) 105708

Contents lists available at ScienceDirect

Catena

journal homepage: www.elsevier.com/locate/catena

Mechanistic understanding of linear erosion under concentrated flow based on laboratory simulations

Jianqiao Han [a,b,*], Binbin Li [c], Guohua Lan [a], Yunyun Dong [a], Wenyan Ge [a,b], Fei Wang [a,b]

[a] Institute of Soil and Water Conservation, Northwest A&F University, Yangling, Shaanxi, China
[b] Institute of Soil and Water Conservation, Chinese Academy of Sciences and Ministry of Water Resources, Yangling, Shaanxi, China
[c] Monitoring Center of Soil and Water Conservation, Ministry of Water Resources, Beijing, China

ARTICLE INFO

Keywords:
Linear erosion
Erosion processes
Flow hydrodynamics
Mechanical mechanisms
Sloped land

ABSTRACT

Elucidating the mechanical mechanisms of linear erosion can contribute to the understanding of soil erosion and its prevention. However, few studies have investigated the development of sediment yield and the mechanical understanding of linear erosion. Experiments, four flow discharge rates and three slope gradients, were conducted for a mechanistic understanding of linear erosion. The conclusions are as follows: (1) The forces that detach soil can be divided into dynamic force (*DF*) and resistance force (*RF*) by vector decomposition and synthesis methods. The difference between *DF* and *RF* is defined as the effective force (*EF*), which represents the comprehensive mechanical effect of soil erosion. (2) DF and RF tend to be balanced during linear erosion. *EF* significantly decreased ($p < 0.05$), *DF* decreased, and *RF* increased. (3) The erosion rate (E_r) decreases noticeably with decreasing *EF* ($p < 0.05$), from 3.99 kg/min to 2.99 kg/min when the slope is 15° and the discharge is 25 L/min. (4) The tendency for mechanical balance is attributed to the interaction among the flow dynamics, resistance, and morphology of linear erosion. The drop-pits and microgeomorphology developed in the linear erosion increased the water flow resistance and decreased the flow dynamics. This mechanical tendency provides a theoretical basis for linear erosion prevention. Our results can help improve the understanding of soil erosion mechanisms and management of water and soil resources.

1. Introduction

Soil erosion leads to topsoil and nutrient loss from slopes and results in land degradation, which threatens the sustainability of the environment and socioeconomic conditions worldwide (Borrelli et al., 2017; Meliho et al., 2019). The transport of excessive quantities of sediment and associated pollutants into hydrological systems leads to sedimentation in rivers and degraded aquatic ecosystem quality (Heng et al., 2011; Lal et al., 2004). Additionally, soil erosion, which can influence CO_2 emissions, plays an important role in the global carbon cycle by enhancing mineralisation and sediment burial (Borrelli et al., 2017; Rosas and Gutierrez, 2019).

Rills, a typical, widely distributed feature of soil erosion, are found in dense occurrences on slopes and represent erosion that occurs as sheet erosion transitions to linear erosion (Qin et al., 2018; Zhang et al., 2016). Sediment yield increases after the formation of rills due to sediment transport that occurs under concentrated flow, which is greater than that under interrill flow (Jiang et al., 2018; Zhao et al., 2018). Rill erosion accounts for >70% of the total sediment yield in rill- and interrill-dominated areas (Qin et al., 2018). Soil erosion increases dramatically if the rill develops into a gully. Many studies have focused on the processes and mechanisms of linear erosion (Di Stefano et al., 2017; Di Stefano et al., 2019; Kimaro et al., 2008; Yang et al., 2018).

Studies have examined soil detachment and sediment transport processes through the hydrodynamic characteristics of runoff (An et al., 2012; Proffitt et al., 1991; Schiettecatte et al., 2008; Shen et al., 2017; Wang et al., 2017). Soil particles detach if the water flow shear stress is greater than the soil critical shear stress (Meyer et al., 1975). Soil detachment can be predicted by various hydraulic parameters, whereas the evolution of rill geometry can only be illustrated by the unit length shear force and shear stress values (Giménez and Govers, 2002). Linear erosion is positively correlated with runoff shear stress, stream power, unit stream power, and energy of the flow section (Shi et al., 2012; Wang et al., 2019).

Rainfall-runoff, topography, soil texture, and surface conditions are the main factors that influence linear erosion by strengthening or

* Corresponding author at: No. 3 Taicheng Road, Institute of Soil and Water Conservation, Northwest A&F University, Yangling, Shaanxi Province, China.
E-mail address: hjq13@163.com (J. Han).

https://doi.org/10.1016/j.catena.2021.105708
Received 18 June 2020; Received in revised form 21 August 2021; Accepted 29 August 2021
Available online 4 September 2021

reducing the erosive ability of runoff and erosion resistance of soil (Chen et al., 2017; Nearing et al., 1997; Sun et al., 2013; Wirtz et al., 2012). Linear erosion primarily results from the detachment and displacement of soil particles influenced by the concentrated flow (Kimaro et al., 2008). Raindrops affect soil erosion by modifying soil surface properties and flow dynamics (Tian et al., 2017). In addition to the slope gradient, roughness, and vegetation conditions, physicochemical properties have critical effects on the resistance to soil erosion (Defersha and Melesse, 2012). On bare slopes, soil particle detachment is driven by multiple forces influenced by rainfall, runoff, and soil characteristics, such as the raindrop impact force (F_R), flow thrust force (F_D), flow uplift force (F_L), soil gravity (G), and soil adhesion force (N) (Ban et al., 2017; Giménez and Govers, 2008). The combined effects of these forces are generalised in the comparison between the flow shear stress and soil critical shear stress, used in the WEPP model (Yang et al., 2018). The critical shear stress, representing the erosion resistance, is often considered to be constant during soil erosion. The same force, which could be decomposed into dynamic and resistance components of soil erosion through detailed mechanical analysis, could generate both promotional and weakening effects on soil detachment. For instance, F_R can be divided into force components perpendicular to the slope, causing friction, and a dynamic component along the direction of water flow, making soil detachment more difficult or easier (Kinnell, 2005). From a mechanical perspective, soil particle detachment and transport are determined by the difference between the dynamic force (*DF*) and the resistance force (*RF*). The difference is defined as the effective force (*EF*), which represents the combined effect of erosion dynamics and resistance.

Although changes in the sediment yield rate and morphology continued during soil erosion, the rate of change substantially decreased after severe erosion, indicating that the linear erosion reached a relatively stable state (He et al., 2017; Shen et al., 2016; Zhang et al., 2018). In the preliminary stage of rill erosion, the sediment yield of the slope was dominated by rill head development. Rill bank collapse and rill bed incision contribute most of the sediment in the middle stage, and the erosion sediment yield exhibits small fluctuations in the later stages of erosion (He et al., 2017). Rainfall-runoff, sediment movement, and erosion morphology constitute a small-scale hydrological geomorphologic system during rill erosion. In this system, rainfall-runoff provides the driving force that influences the sediment transport, runoff changes, infiltration, flow dynamics, and sediment yield processes, and then changes the morphology of linear erosion (Brunton and Bryan, 2000; Zhang et al., 2017).

Studies have mainly focused on linear erosion and its dynamic mechanisms. However, few studies have investigated the development of sediment yield and the mechanical understanding of linear erosion. The evolution of the sediment yield and morphology results from the mutual adaptation between rainfall and runoff dynamics and slope surface characteristics. Because the runoff and slope mutually adapt, the mechanical relationship between the *DF* and *RF* is worth exploring during linear erosion. Further studies are necessary to investigate the changes in the mechanical features and their effects on linear erosion.

The objectives of this study are as follows: (i) investigate the changes in the mechanical indices (*DF, RF,* and *EF*) and their mechanical relationships and (ii) assess the effects of mechanical changes on the sediment yield in linear erosion. These results improve the understanding of linear erosion, promote physical process models, and thus advance the practice of soil erosion prevention.

2. Materials and methods

2.1. Experimental materials

The experiments were performed in an artificial rainfall hall at the Institute of Soil and Water Conservation, Chinese Academy of Sciences and Ministry of Water Resources, Yangling, Shaanxi, China. Concentrated flow experiments were conducted in a flume in which the slope angle could be adjusted from 0% to 30%. The length, width, and depth measurements of the flume are 3.0 m, 1.0 m, and 0.8 m, respectively (Fig. 1).

2.2. Experimental design

To simulate the typical linear erosion under concentrated flows, 12 treatments combined with four flow discharges and three slope gradients were conducted. The flow discharges of 10, 15, 20, and 25 L min^{-1} were equivalent to rainfall intensities of 60, 90, 120, and 150 mm h^{-1} exerted on a slope (10 m × 1 m), according to the erosional rainfall standards from the Loess Plateau (Qin et al., 2018; Tian et al., 2017). The equivalent rainfall intensities of 60, 90, 120, and 150 mm h^{-1} on slopes (10 m × 1 m) were 200, 300, 400, and 500 mm h^{-1} on the flume (3 m × 1 m), respectively. Three slope gradients were designed: 10°, 15°, and 20° (Ban et al., 2017; Qin et al., 2018). Using the characteristics of soil erosion caused by a rainstorm, the duration of each treatment was 1 h (Tian et al., 2017). Two duplicate runs were conducted for each treatment.

2.3. Experimental procedures

A 10-cm-thick layer of natural fine sand was emplaced on the flume bottom before filling the flume with soil. The top 70 cm of the flume was filled with soil in 5 cm increments, and the soil bulk density was 1.20 g cm^{-3}. To separate the sand and soil layers, a highly permeable cloth was placed on the sand layer. During the soil filling process, the soil amount of each layer (5 cm) was kept as constant as possible to maintain a uniform soil bulk density in the flume (Zhang et al., 2017). By using the same soil texture and surface smoothing methods, the roughness of the slope surface in each experimental run was approximated before releasing concentrated flows. The transition area between the water-supplying tank and the flume was covered with gravel to stabilise the bare soil and flow.

To make the soil saturation uniform, consolidate the soil particles, and reduce the spatial variability in the soil conditions, 30-mm h^{-1} of pre-rain treatment was conducted in the soil flume set at a 3° gradient until runoff was generated on the surface. After the pre-rain treatment, a plastic film covered the soil surface to prevent soil moisture loss and improve surface sealing (Qin et al., 2018).

The flume was set at the designed gradient to conduct the experiments 24 h after the pre-rain event. Subsequently, inflow discharges were calibrated to the target discharge with a relative error of less than 5%. After releasing the concentrated flows, the runoff and sediments were sampled at the flume outlet at 5 min intervals.

Five cross-sections, 0.5, 1.0, 1.5, 2.0, 2.5 m from the flume crest, were set up to measure the velocity of the surface flow by the $KMnO_4$ dye-tracing method three times. The mean flow velocity was obtained by multiplying the surface velocity by 0.75; next, the result was averaged to represent the flow velocity of the entire linear erosion channel (Shen et al., 2016). The flow depth and width were measured using a gauge pin and steel ruler three times, respectively (Peng et al., 2015). The sediment concentration was measured by oven-drying, and the erosion rate (E_r) was calculated based on the time, runoff, and sediment concentration.

2.4. Calculation of DF, RF, and EF

According to the mechanical theory of object motion, the force structure of the soil particles under concentrated flow conditions was established (Fig. 2). The forces include F_D, F_L, G, N, and f. f is the frictional force caused by the pressure vertical to the slope. The meanings of all abbreviations are listed in Table S1.

A rectangular coordinate system was established with the x-axis parallel to the slope direction and the y axis perpendicular to the slope direction. The dynamic and resistance components of each force acting

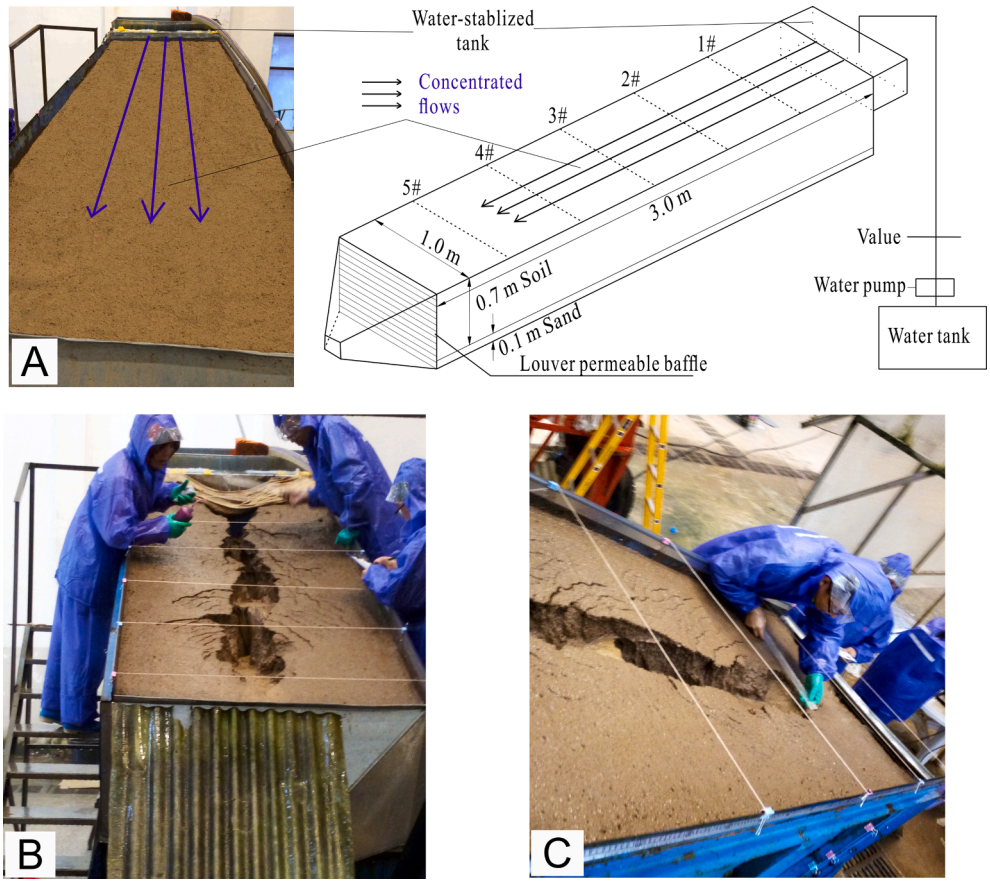

Fig. 1. Records of the experimental processes and sketch of the facilities. A: Initial slope without erosion and sketch of the facilities; B: Linear erosion photographed from the end of the flume; and C: Linear erosion photographed from the upper right of the flume.

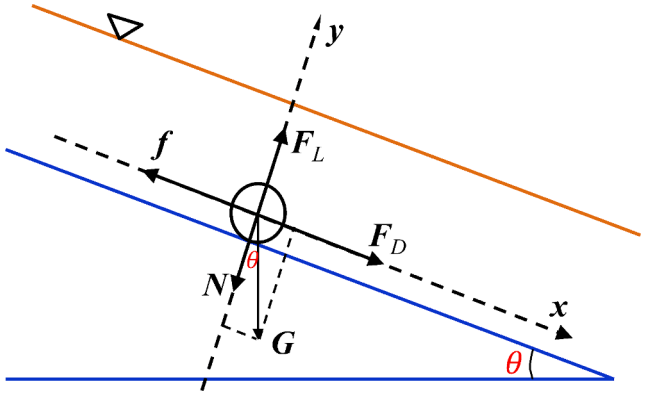

Fig. 2. Force analysis schematic of the soil particles under concentrated flows.

on the soil particle movement along the x-axis were analysed using vector decomposition and synthesis methods. The difference between the dynamic and resistance components characterises the *EF of* soil erosion. The *RF* is caused by the pressure vertical to the slope in the current generalisation system. Analysis results of the effective slope erosivity at slope angle θ are listed in Table 1, where φ is the underwater repose angle of the soil particles, and tanφ is the slope friction coefficient. For natural soil, tanφ is quantified as 0.63 (Zhao et al., 2013).

According to the aforementioned analysis, *DF*, *RF*, and *EF* in linear erosion are calculated as follows:

$$DF = F_D + Gsin\theta \tag{1}$$

Table 1
Analysis of the *DF*, *RF*, and *EF* components of each force.

Force source	Force	*DF* component	*RF* component	*EF* component
Water flow	F_D	F_D	0	F_D
	F_L	0	$-F_L \tan\varphi$	$F_L \tan\varphi$
Soil	G	$G \sin\theta$	$G \cos\theta \tan\varphi$	$G \sin\theta – G \cos\theta \tan\varphi$
	N	0	$N \tan\varphi$	$-N \tan\varphi$

$$RF = (Gcos\theta + N - F_L)tan\varphi \tag{2}$$

$$EF = F_D + Gsin\theta - (Gcos\theta + N - F_L)tan\varphi \tag{3}$$

The calculation methods of G, F_D, and F_L are as follows:

$$\begin{cases} G = (\rho_s - \rho)g\dfrac{\pi}{6}d^3 \\ F_D = C_x\dfrac{\pi}{4}d^2\dfrac{\rho v^2}{2} \\ F_L = C_y\dfrac{\pi}{4}d^2\dfrac{\rho v^2}{2} \end{cases} \tag{4}$$

where ρ_s is the density of sand (1650 kg/m^3); ρ is the density of water (1000 kg/m^3); g is the acceleration due to gravity (9.8 m/s^2); *and* C_x and C_y are the drag coefficients of thrust (0.7) and lift (0.18), respectively (Zhang, 1998). d is the median soil particle size (m), and v is the flow velocity (m/s).

N, which represents the adhesion effects in cohesive soil, was calculated using Tang Cunben's equation, as follows:

$$N = d(\gamma'_s/\gamma'_{s,c})^{10}\delta_c \quad (5)$$

where d is the soil particle size; and γ'_s and $\gamma'_{s,c}$ are the dry bulk density (1.2 g/cm^3) and stable dry bulk densities (1.6 g/cm^3), respectively. $\hat{I}_c$ is the cohesion coefficient, quantified as 0.915×10^{-4} (Zhang, 1998).

2.5. Data analysis methods

In this study, data series normality was assessed using the Kolmogorov–Smirnov test. The method first compares the sample cumulative density measured in a specific field with the assumed sample distribution function (the normal distribution in our case) and then tests whether the deviation of the two functions satisfies the significance requirements. When the observed value is greater than equal to the critical value of the Kolmogorov–Smirnov statistics at 95% significance requirements, the hypothesis of a normal distribution is rejected (Zhang et al., 2006).

In our study, simple linear regression was used to test the statistical significance of the correlation between the erosion intensities (mechanical parameters) and discharge durations. A probability (p) value $<$ 0.05 was considered statistically significant (Han et al., 2019; Peng et al., 2015). The parametric t-test comprises two steps: first, a simple linear regression equation was fit, in which time t is considered to be the independent variable and an erosion variable (E_r or EF) is considered to be the dependent variable; second, the statistical significance of the slope of the regression equation was tested.

3. Results

The Kolmogorov–Smirnov test demonstrates that the time series of E_r, EF, RF, and DF values under the 12 treatments are normally distributed, indicating that linear regression is reliable. The results of the trend analysis of the sediment yield and mechanical parameters are presented in the following sections.

3.1. Changes in the sediment yield during linear erosion

The E_r values of the rills/gullies under different treatments are shown in Fig. 3. At the specified slope gradient, E_r increases as discharge increases. The average value of E_r increases from 1.65 kg/min at 10 L/min to 2.97 kg/min at 25 L/min when the slope is 15°. Analogously, E_r increased as the slope gradient increased at a specified discharge. Notably, the regression equation between E_r and t reflects a decrease in E_r during linear erosion (Table 2). For instance, E_r decreases from 3.99 kg/min to 2.99 kg/min when the slope is 15°, and the discharge is 25 L/min. There was a remarkable decrease in sediment yield during linear erosion under concentrated flows ($p < 0.05$).

3.2. Changes in the flow velocity during linear erosion

Fig. 4 shows the temporal changes in the flow velocity for typical linear erosion under different treatments. In general, the flow velocity decreased rapidly first and then gradually stabilised with soil erosion time under different treatments, where the velocity decreased dramatically before 30 min and reached a fluctuating state after 30 min. Specifically, the flow velocity decrease from 0.31 m/s at 5 min to 0.19 m/s at 30 min; however, the velocity ranges from 0.18 to 0.20 during the 30 to 60 min when the slope was 15° and runoff was 20 L/min. The flow velocity exhibits an increasing trend with concentrated flows. The flow velocities are 0.19, 0.20, 0.22, and 0.24 m/s, when the slope is 10° and the time is 25 min. Analogously, these change features also exist in a typical linear erosion process under other treatments.

3.3. Changes in the mechanical parameters during linear erosion

Fig. 5 shows the changes in the DF and RF that occur during typical linear erosion. DF and RF exhibited inverse change trends as linear erosion. A decrease in DF occurs while an increase emerges in the RF, promoting equilibration between DF and RF. In Fig. 6 and Table 3, both the images and data show that the DF and RF tend to balance as EF gradually decreases. Therefore, the dynamic and resistance components of the forces tend to balance during linear erosion.

3.4. Relationship between E_r and EF

To reveal the relationship between E_r and EF, 144 sets of E_r and EF in the 12 treatments were displayed over time (Fig. 7). In Fig. 7A, the data points are grouped based on the slope gradient (10°, 15°, and 20°) to reflect the relationship between them. To further verify this relationship, data were organised by the four discharge amounts (10, 15, 20, and 25 L min^{-1}; Fig. 7B). The R^2 of the regression equation between E_r and EF was 0.81, indicating that there was a significant linear correlation between the erosion intensity and the mechanical index ($p < 0.05$). In brief, linear erosion is driven by the EF. The larger the EF, the higher the erosion intensity.

4. Discussion

4.1. Mechanical change and its effects on linear erosion

The results show that DF decreases and RF increases with linear erosion under concentrated flows, and the dynamic and resistance forces tend to be balanced, indicating that a mechanical tendency exists during linear erosion. These results are consistent with those of studies on the dynamic mechanics of rill erosion (Shen et al., 2016; Zhang et al., 2018). For example, hydrodynamic parameters remain relatively stable during the later stages of rill erosion (He et al., 2017). At smaller slopes (≤15°), rill erosion and flow velocity quickly reached a steady-state; when the slope gradient was high (≥20°), the unsteady rill erosion period was maintained for a long time because of the strong erosion, resulting in a fluctuating decrease in flow velocity in the active period of rill erosion (He et al., 2017). The flow hydrodynamic parameters first increased and

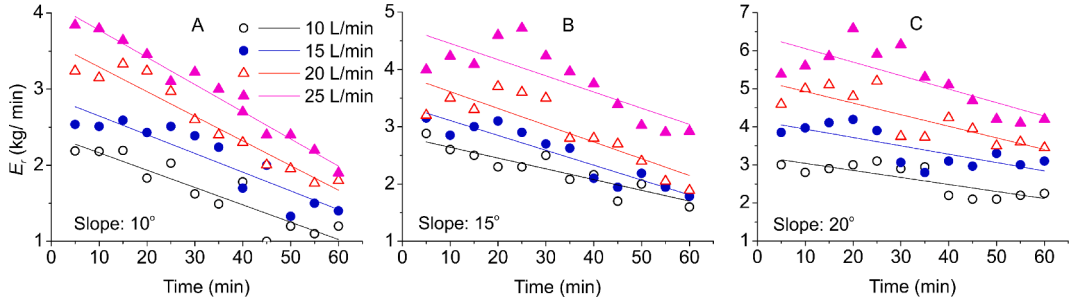

Fig. 3. Temporal changes in E_r of the linear erosion under different treatments. A: Slope gradient of 10°; B: Slope gradient of 15°; and C: Slope gradient of 20°. The statistical values and their significance are shown in Table 2.

Table 2
Regression analysis equation between E_r and time (t).

Discharge (L/min)	10°			15°			20°		
	Equation	R^2	p	Equation	R^2	p	Equation	R^2	p
10	$E_r = -0.0228\ t + 2.39$	0.84	0.00	$E_r = -0.0188\ t + 2.83$	0.82	0.00	$E_r = -0.0185\ t + 3.23$	0.66	0.00
15	$E_r = -0.0246\ t + 2.89$	0.83	0.00	$E_r = -0.0260\ t + 3.37$	0.88	0.00	$E_r = -0.0225\ t + 4.16$	0.60	0.00
20	$E_r = -0.0324\ t + 3.61$	0.93	0.00	$E_r = -0.0293\ t + 3.90$	0.74	0.00	$E_r = -0.0305\ t + 5.23$	0.68	0.00
15	$E_r = -0.0357\ t + 4.13$	0.98	0.00	$E_r = -0.0282\ t + 4.74$	0.66	0.00	$E_r = -0.0355\ t + 6.41$	0.61	0.00

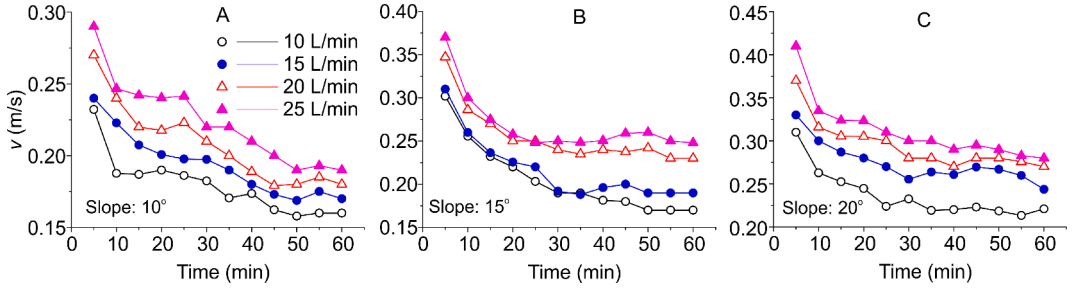

Fig. 4. Temporal changes in flow velocity of the linear erosion under the different treatments. A: Slope gradient of 10°; B: Slope gradient of 15°; and C: Slope gradient of 20°.

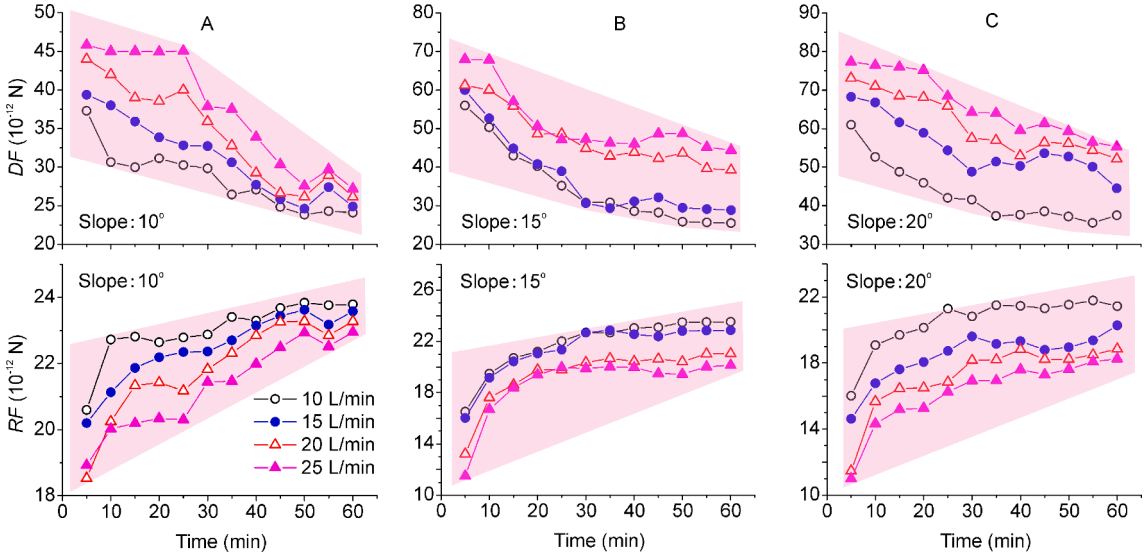

Fig. 5. Temporal changes in *DF* and *RF* of the linear erosion under the different treatments. A: Slope gradient of 10°; B: Slope gradient of 15°; and C: Slope gradient of 20°.

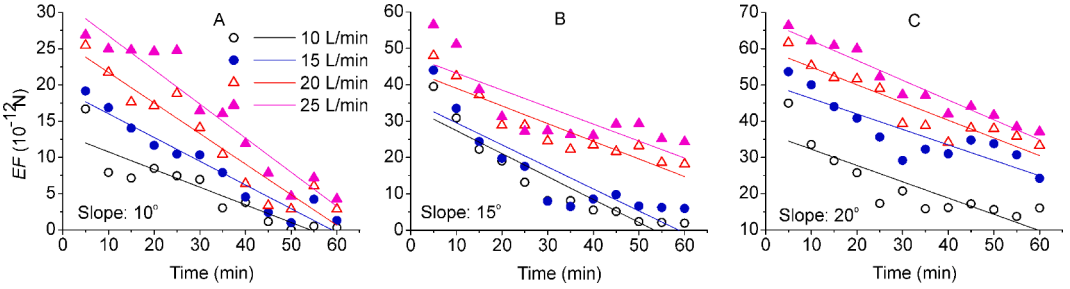

Fig. 6. Temporal changes in *EF* of the linear erosion under the different treatments. A: Slope gradient of 10°; B: Slope gradient of 15°; and C: Slope gradient of 20°. The statistical values and their significance are shown in Table 3.

Table 3
Regression analysis equation between *EF* and time (t).

Discharge (L/min)	10°			15°			20°		
	Equation	R^2	p	Equation	R^2	p	Equation	R^2	p
10	$EF = -0.2438\ t + 13.21$	0.82	0.00	$EF = -0.6317\ t + 33.71$	0.86	0.00	$EF = -0.4490\ t + 36.76$	0.73	0.00
15	$EF = -0.3276\ t + 19.31$	0.93	0.00	$EF = -0.6057\ t + 35.59$	0.77	0.00	$EF = -0.4266\ t + 50.53$	0.77	0.00
20	$EF = -0.4216\ t + 25.94$	0.91	0.00	$EF = -0.4858\ t + 43.89$	0.84	0.00	$EF = -0.4882\ t + 59.793$	0.87	0.00
15	$EF = -0.4706\ t + 31.49$	0.93	0.00	$EF = -0.4674\ t + 47.88$	0.63	0.00	$EF = -0.5460\ t + 67.67$	0.95	0.00

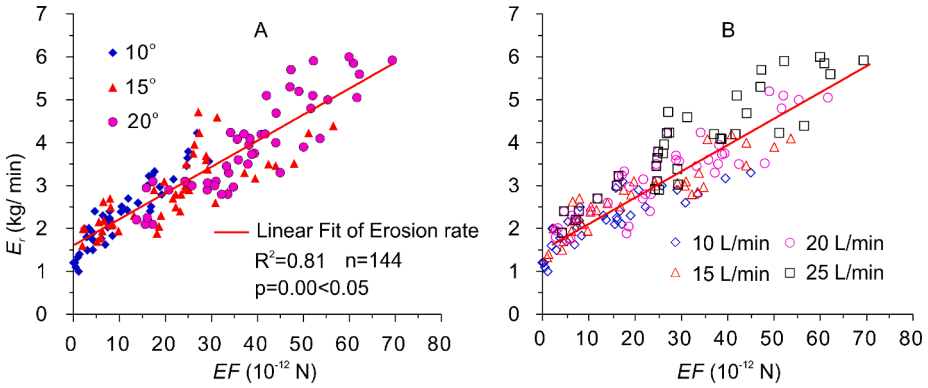

Fig. 7. Relationship between E_r and *EF*. A: Data points are grouped by slope gradient; B: Data points are grouped by discharge.

then decreased with soil erosion (Qin et al., 2018).

The relationship between *EF* and E_r indicates that the effective eroding force is the driving factor for soil separation and transportation, and a reduction in the effective erosivity causes the soil erosion to decrease. Studies have demonstrated that the sediment yield of the rills first increases and then remains stable or fluctuates within a certain range (Qin et al., 2018). According to the intensity of the sediment yield, the rill erosion was divided into the initial stage, development stage, and stabilisation stage, among which the sediment yield in the development stage was the highest, and that in the stabilisation stage was the lowest when the rill was in a steady-state (Hao et al., 2017). He et al. (2017) divide rill erosion into three stages (A, B, and C) according to rainfall duration stages. The runoff rate fluctuated in stages A and B and was relatively stable in stage C; the sediment concentration slowly increased in stage A, sharply increased in stage B, and remained stable in stage C.

Unlike the results in the literature, our results reveal a tendency for mechanical changes during typical linear erosion, leading to a fluctuating decrease in sediment erosion.

4.2. Causes of the mechanical tendency

The feedback effect of the linear erosion morphology on the flow dynamics is the main cause of the mechanical adjustment during linear erosion. Zhang et al. (2017) posit that the rills formed by rainfall-runoff on the slope are not only the sediment transport channels but also the sources of erosion sediment, leading to rill morphology changes. In Fig. 1B, the cross-sections of the linear erosion channel were inconsistent along the slope, and the channel depths were small at several points. After the pre-rain treatment, the slope underlying the surface, which has a uniform soil texture and ability to saturate, is not the cause of inhomogeneity in the cross-sections. According to another study, scour ability decreases because of the increasing sediment concentration in the concentrated flow (Qin et al., 2018). Along with the numerous random drop-pits that prevent the flow, the changing scour capacities of the flow result in the inhomogeneous shape of the sections, increasing the morphology resistance of the linear erosion channel to the flow. In addition, drop-pits with large slope gradients increase the morphological resistance of the linear erosion channel, dissipate the flow energy, and then weaken the erosion dynamics (Giménez and Govers, 2001). The flow velocity decreases because of a series of steep ridges and depressions along the rill bed (Giménez et al., 2004). Moreover, a rill flow depth of centimetre scale or shallower leads to flow dynamics that are easily affected by the bed morphology (Lei et al., 1998; Stefanovic and Bryan, 2009). As scouring continues, more drop-pits are formed in the linear bed, increasing the morphology resistance (Zhao et al., 2017).

In addition to the drop-pit, linear erosion channel widening and bending have distinct effects on flow dynamics. Because channel walls constantly collapse, the flow paths along the channel bed become tortuous and winding, and the shape resistance of the channel bed increases, resulting in a decrease in the flow velocity (Stefanovic and Bryan, 2009). During linear erosion, the main erosion pattern changed from channel bed incision to channel bank collapse, and the random accumulation of collapses increased the flow depth and width, reducing the flow velocity (Qin et al., 2019; Wells et al., 2013). The increasing resistance induced by linear erosion morphology changes is consistent with our result that the *RF* increased during linear erosion (Fig. 5).

There is an interaction between flow dynamics and rill morphology in rill erosion (Zhang et al., 2016). The flow velocity changes the rill morphology through sand migration and energy exchange, and the changing rill shape affects the water flow hydraulics through bed roughness adjustment (Giménez and Govers, 2001). Therefore, the changes in flow hydraulics correspond to the evolution of continuous microtopography during typical linear erosion. With linear erosion, microgeomorphological adjustments result in an increase in flow resistance and a decrease in flow dynamics.

4.3. Implications of the mechanical tendency on soil erosion prevention

According to the relationship between the effective eroding force and sediment yield, the mechanical tendency is the theoretical basis for linear erosion prevention. With appropriate strategies, linear erosion can be weakened by promoting the mechanical tendency between erosion dynamics and resistance. For instance, vegetation restoration and straw mulching increase erosion resistance and reduce flow power (Rahma et al., 2017), accelerating the mechanical tendency in linear erosion. Based on the operation of the drainage facilities, the flow dynamics decrease because of decreases in the runoff on the slope. Therefore, erosion is weakened by the mechanical relationship between

the erosion ability of runoff and the erosion resistance of the soil. Moreover, strategies such as conservation tillage can be used to improve soil structure and increase soil erosion resistance (Jia et al., 2019; Langhans et al., 2019). Overall, prevention methods that promote mechanical tendencies would reduce soil loss during linear erosion.

In addition, the mechanical tendency enhances the understanding of the linear erosion mechanisms, which can be used to promote physically based erosion models. Improving the understanding of linear erosion mechanisms and developing models and prevention methods would reduce soil erosion and associated land degradation, aquatic ecosystem deterioration, and global carbon emissions.

5. Conclusions

We present a systematic investigation of the mechanical understanding of typical linear erosion by using simulation experiments. The forces that detach soil, such as *FD, FL, G, N*, and *f*, can be divided into *DF* and *RF* by vector decomposition and synthesis methods. A mechanical tendency occurs during linear erosion under concentrated flow. With linear erosion, the decrease in *DF* and increase in *RF* induced a significant decrease in *EF* ($p < 0.05$). The linear relationship between E_r and *EF* was quite significant ($p < 0.05$); decreasing the *EF* resulted in the stabilisation of the sediment yield. The feedback effects of the development of microgeomorphology caused by runoff increase the flow resistance and decrease the flow dynamics. The interactions among flow dynamics, resistance, and linear erosion morphology result in a mechanical tendency that occurs during linear erosion. These findings contribute to the understanding of the development of linear erosion and its mechanical mechanisms. To some extent, soil loss can be controlled through prevention strategies that promote mechanical balance. The consideration of mechanical tendencies would improve the physically based erosion models, which could be used in basin management.

This study provides a generalised analysis of the mechanical mechanism. Unstructured soil and concentrated flows without a raindrop were used to verify the hypothesis on the mechanical tendency in the laboratory simulations of linear erosion. Extending these findings requires further research that considers, for example, the original soil, raindrop, rill/gully network, and changing calculation parameters.

Declaration of Competing Interest

The authors declare that they have no known competing financial interests or personal relationships that could have appeared to influence the work reported in this paper.

Acknowledgements

This work was supported by the National Natural Science Foundation of China [grant numbers 41807067, 41771558, 41907061]; the Water and Soil Conservancy Science Plan in Shaanxi Province of China [grant number 2017sbkj-01]; the Youth Talent Lift Project of China Association for Science and Technology [grant number 2019-2021QNRC001].

Appendix A. Supplementary material

Supplementary data to this article can be found online at https://doi.org/10.1016/j.catena.2021.105708.

References

An, J., Zheng, F., Lu, J., Li, G., 2012. Investigating the role of raindrop impact on hydrodynamic mechanism of soil erosion under simulated rainfall conditions. Soil Sci. 177, 517–526.
Ban, Y.Y., Lei, T.W., Liu, Z.Q., Chen, C., 2017. Comparative study of erosion processes of thawed and non-frozen soil by concentrated meltwater flow. Catena 148, 153–159.
Borrelli, P., Robinson, D.A., Fleischer, L.R., Lugato, E., Ballabio, C., Alewell, C., Meusburger, K., Modugno, S., Schütt, B., Ferro, V., Bagarello, V., Oost, K.V., Montanarella, L., Panagos, P., 2017. An assessment of the global impact of 21st century land use change on soil erosion. Nat. Commun. 8, 2013.
Brunton, D.A., Bryan, R.B., 2000. Rill network development and sediment budgets. Earth Surf. Proc. Land. 25 (7), 783–800.
Chen, X.-Y., Huang, Y.-H., Zhao, Y., Mo, B., Mi, H.-X., Huang, C.-H., 2017. Analytical method for determining rill detachment rate of purple soil as compared with that of loess soil. J. Hydrol. 549, 236–243.
Defersha, M.B., Melesse, A.M., 2012. Effect of rainfall intensity, slope and antecedent moisture content on sediment concentration and sediment enrichment ratio. Catena 90, 47–52.
Di Stefano, C., Ferro, V., Palmeri, V., Pampalone, V., 2017. Flow resistance equation for rills. Hydrol. Process. 31 (15), 2793–2801.
Di Stefano, C., Nicosia, A., Pampalone, V., Palmeri, V., Ferro, V., 2019. New technique for measuring water depth in rill channels. Catena 181, 104090. https://doi.org/10.1016/j.catena.2019.104090.
Giménez, R., Govers, G., 2001. Interaction between bed roughness and flow hydraulics in eroding rills. Water Resour. Res. 37 (3), 791–799.
Giménez, R., Govers, G., 2002. Flow detachment by concentrated flow on smooth and irregular beds. Soil Sci. Soc. Am. J. 66 (5), 1475–1483.
Giménez, R., Govers, G., 2008. Effects of freshly incorporated straw residue on rill erosion and hydraulics. Catena 72 (2), 214–223.
Giménez, R., Planchon, O., Silvera, N., Govers, G., 2004. Longitudinal velocity patterns and bed morphology interaction in a rill. Earth Surf. Proc. Land. 29 (1), 105–114.
Han, J., Gao, J., Luo, H., 2019. Changes and implications of the relationship between rainfall, runoff and sediment load in the wuding river basin on the chinese loess plateau. Catena 175, 228–235.
Hao, H., Guo, Z., Wang, X., Zhan, H., Ma, R., Li, Z., Jiang, J., 2017. Rill erosion process on red soil slope under interaction of rainfall and scouring flow. Trans. Chinese Soc. Agric. Eng. 33, 134–140.
He, J.-J., Sun, L.-Y., Gong, H.-l., Cai, Q.-G., 2017. Laboratory studies on the influence of rainfall pattern on rill erosion and its runoff and sediment characteristics. Land Degrad. Dev. 28 (5), 1615–1625.
Heng, B.C.P., Sander, G.C., Armstrong, A., Quinton, J.N., Chandler, J.H., Scott, C.F., 2011. Modeling the dynamics of soil erosion and size-selective sediment transport over nonuniform topography in flume-scale experiments. Water Resour. Res. 47 (2) https://doi.org/10.1029/2010WR009375.
Jia, L., Zhao, W., Zhai, R., Liu, Y., Kang, M., Zhang, X., 2019. Regional differences in the soil and water conservation efficiency of conservation tillage in china. Catena 175, 18–26.
Jiang, F., Zhan, Z., Chen, J., Lin, J., Wang, M.K., Ge, H., Huang, Y., 2018. Rill erosion processes on a steep colluvial deposit slope under heavy rainfall in flume experiments with artificial rain. Catena 169, 46–58.
Kimaro, D.N., Poesen, J., Msanya, B.M., Deckers, J.A., 2008. Magnitude of soil erosion on the northern slope of the uluguru mountains, tanzania: interrill and rill erosion. Catena 75 (1), 38–44.
Kinnell, P.I.A., 2005. Raindrop-impact-induced erosion processes and prediction: a review. Hydrol. Process. 19 (14), 2815–2844.
Lal, R., Griffin, M., Apt, J., Lave, L., Morgan, M., 2004. Managing soil carbon. Science 304, 393.
Langhans, C., Diels, J., Clymans, W., Van den Putte, A.n., Govers, G., 2019. Scale effects of runoff generation under reduced and conventional tillage. Catena 176, 1–13.
Lei, T., Nearing, M.A., Haghighi, K., Bralts, V.F., 1998. Rill erosion and morphological evolution: a simulation model. Water Resour. Res. 34 (11), 3157–3168.
Meliho, M., Nouira, A., Benmansour, M., Boulmane, M., Khattabi, A., Mhammdi, N., Benkdad, A., 2019. Assessment of soil erosion rates in a mediterranean cultivated and uncultivated soils using fallout 137cs. J. Environ. Radioact. 208-209, 106021. https://doi.org/10.1016/j.jenvrad.2019.106021.
Meyer, L.D., Foster, G.R., Nikolov, S., 1975. Effect of flow rate and canopy on rill erosion. Trans. Asae 18, 905–911.
Nearing, M.A., Norton, L.D., Bulgakov, D.A., Larionov, G.A., West, L.T., Dontsova, K.M., 1997. Hydraulics and erosion in eroding rills. Water Resour. Res. 33 (4), 865–876.
Peng, W., Zhang, Z., Zhang, K., 2015. Hydrodynamic characteristics of rill flow on steep slopes. Hydrol. Process. 29 (17), 3677–3686.
Proffitt, A.P.B., Rose, C.W., Hairsine, P.B., 1991. Rainfall detachment and deposition: experiments with low slopes and significant water depths. Soil Sci. Soc. Am. J. 55, 325–332.
Qin, C., Zheng, F., Wilson, G.V., Zhang, X.J., Xu, X., 2019. Apportioning contributions of individual rill erosion processes and their interactions on loessial hillslopes. Catena 181, 104099. https://doi.org/10.1016/j.catena.2019.104099.
Qin, C., Zheng, F., Zhang, X.J., Xu, X., Liu, G., 2018. A simulation of rill bed incision processes in upland concentrated flows. Catena 165, 310–319.
Rahma, A.E., Wei, W., Tang, Z., Lei, T., Zhao, J., 2017. Straw mulch can induce greater soil losses from loess slopes than no mulch under extreme rainfall conditions. Agric. For. Meteorol. 232, 141–151.
Rosas, M.A., Gutierrez, R.R., 2019. Assessing soil erosion risk at national scale in developing countries: the technical challenges, a proposed methodology, and a case history. Sci. Total Environ. 135474.
Schiettecatte, W., Verbist, K., Gabriels, D., 2008. Assessment of detachment and sediment transport capacity of runoff by field experiments on a silt loam soil. Earth Surf. Proc. Land. 33, 1302–1314.
Shen, H., Zheng, F., Wen, L., Yong, H., Wei, H., 2016. Impacts of rainfall intensity and slope gradient on rill erosion processes at loessial hillslope. Soil Tillage Res. 155, 429–436.
Shen, N., Wang, Z., Zhang, Q., Wu, B., Wang, D., Zhang, Q., Liu, J.E., 2017. Quantifying the contribution of sediment load to soil detachment rate by sediment-laden rill flow. Soil Sci. Soc. Am. J. 81, 1526–1536.

Shi, Z.H., Fang, N.F., Wu, F.Z., Wang, L., Yue, B.J., Wu, G.L., 2012. Soil erosion processes and sediment sorting associated with transport mechanisms on steep slopes. J. Hydrol. 454–455, 123–130.
Stefanovic, J.R., Bryan, R.B., 2009. Flow energy and channel adjustments in rills developed in loamy sand and sandy loam soils. Earth Surf. Proc. Land. 34, 133–144.
Sun, L., Fang, H., Deli, Q.I., Junlan, L.I., Cai, Q., 2013. A review on rill erosion process and its influencing factors. Chinese Geogr. Sci. 23, 389–402.
Tian, P., Xu, X., Pan, C., Hsu, K., Yang, T., 2017. Impacts of rainfall and inflow on rill formation and erosion processes on steep hillslopes. J. Hydrol. 548, 24–39.
Wang, Y., Cao, L., Fan, J., Lu, H., Zhu, Y., Gu, Y., Sun, B., Liang, Y., 2017. Modelling soil detachment of different management practices in the red soil region of china. Land Degrad. Dev. 28, 1496–1505.
Wang, Y., Luo, J., Zheng, Z., Li, T., He, S., Zhang, X., Wang, Y., Liu, T., 2019. Assessing the contribution of the sediment content and hydraulics parameters to the soil detachment rate using a flume scouring experiment. Catena 176, 315–323.
Wells, R.R., Momm, H.G., Rigby, J.R., Bennett, S.J., Bingner, R.L., Dabney, S.M., 2013. An empirical investigation of gully widening rates in upland concentrated flows. Catena 101, 114–121.
Wirtz, S., Seeger, M., Ries, J.B., 2012. Field experiments for understanding and quantification of rill erosion process. Catena 91, 21–34.
Yang, D., Gao, P., Zhao, Y., Zhang, Y., Liu, X., Zhang, Q., 2018. Modeling sediment concentration of rill flow. J. Hydrol. 561, 286–294.
Zhang, P., Yao, W., Tang, H., Wei, G., Wang, L., 2017. Laboratory investigations of rill dynamics on soils of the loess plateau of china. Geomorphology 293, 201–210.
Zhang, P., Zhang, N., Tang, H., Yao, W., Xizhi, L.V., 2016. Experimental investigation of morphological characteristics of rill evolution on loess slope. Catena 137, 536–544.
Zhang, Q., Liu, C., Xu, C., Xu, Y., Jiang, T., 2006. Observed trends of annual maximum water level and streamflow during past 130 years in the yangtze river basin, china. J. Hydrol. 324, 255–265.
Zhang, R., 1998. Fluvial sediment dynamics. China WaterPower Press, Beijing, pp. 63–67.
Zhang, X., Li, P., Li, Z.B., Yu, G.Q., Li, C., 2018. Effects of precipitation and different distributions of grass strips on runoff and sediment in the loess convex hillslope. Catena 162, 130–140.
Zhao, B.S., Wang, S.X., Kui, X.U., Zhen, X.U., Wang, P.F., 2017. Experimental study of drop pit characteristics of rill erosion on foreland pluvial fan slopeland. Arid Land Geogr. 40, 348–354.
Zhao, C., Gao, J.E., Shao, H., Wang, H., Xu, X., 2013. Numerical simulation of runoff generation and sediment transport processes under different lands use patterns. J. Sichuan Univ. (Eng. Sci. Ed.) 45, 38–46.
Zhao, L., Hou, R., Wu, F., 2018. Effect of tillage on soil erosion before and after rill development. Land Degrad. Dev. 29, 2506–2513.